NANO LETTERS

pubs.acs.org/NanoLett Letter

Metaoptronic Multiplexed Interface for Probing Bioentity Behaviors

Li Zhang, Quanying Fu, Yayin Tan, Xuemeng Li, Yanhui Deng, Zhang-Kai Zhou,* Bin Zhou, Hongqi Xia, Huanjun Chen, Cheng-Wei Qiu,* and Jianhua Zhou*

Cite This: *Nano Lett.* 2021, 21, 2681−2689 Read Online

ACCESS | Metrics & More | Article Recommendations | Supporting Information

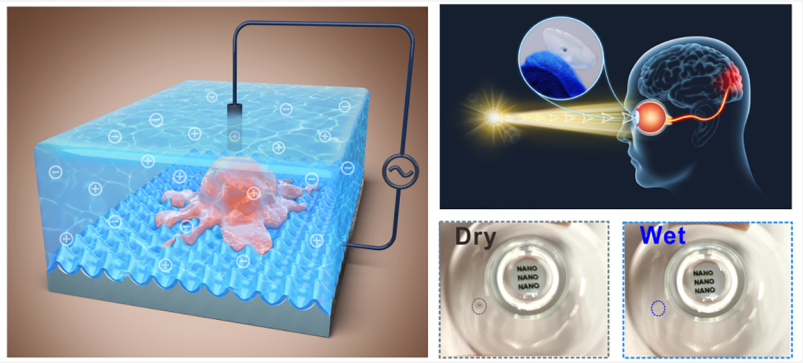

ABSTRACT: Biointerface sensors have brought about remarkable advances in modern biomedicine. To accurately monitor bioentity's behaviors, biointerface sensors need to capture three main types of information, which are the electric, spectroscopic, and morphologic signals. Simultaneously obtaining these three types of information is of critical importance in the development of future biosensor, which is still not possible in the existing biosensors. Herein, by synergizing metamaterials, optical, and electronic sensing designs, we proposed the metaoptronic multiplexed interface (MMI) and built a MMI biosensor which can collectively record electric, spectroscopic, and morphologic information on bioentities. The MMI biosensor enables the real-time triple-monitoring of cellular dynamics and opens up the possibility for powerlessly monitoring ocular dryness. Our findings not only demonstrate an advanced multiplexed biointerface sensor with integrated capacities but also help to identify a uniquely significant arena for the nanomaterials, meta-optics, and nanotechnologies to play their roles in a complementary manner.

KEYWORDS: *multiplexed biosensor, colorless sensor, complementary triple-monitoring, powerlessly ocular sensing*

Biosensors have been widely employed to monitor the activities of a living body, which have brought about great advances for early diagnosis, smart medicine, and healthcare monitoring with wearable technologies.[1−4] As a significant class of biosensor, biointerface sensors focus on the bioentity's interfacial behaviors such as molecular recognition, biochemical reaction, cellular deformation, microenvironmental change, and so forth. These sensors accurately reveal the existence, compatibility, activity, and biological status of bioentities during their interactions with external materials.[5−8] In addition, the biointerface sensors also serve as the core devices for transforming biological information from the biointerface into digitally readable signals, shedding light on the development of implantable devices, human-computer interaction (HCI), smart wearable devices, and so forth.[9−12]

Generally, the biointerface sensors are required to collect three important types of information, which are the electric, spectroscopic, and morphologic signals. To be specific, on the basis of electric changes (such as the impedance or resistance variation), the electric sensors can detect the electron transfer processes of ions or biomolecules hereby revealing their adsorbing or transferring dynamics.[13] Those electric biointerface sensors usually have advantages of low-cost, high selectivity, and easy integration, enabling their wide applications both in lab and commercial market. For example, over 90% of the commercial home-testing glucometers, manufactured by the four major companies (i.e., Life Scan, Roche Diagnostic, Abbott, and Bayer), are based on the electrochemical sensor strips. In addition, in a biosystem the characteristic spectral profiles (i.e., position and intensity of resonance peaks) can provide rich information about molecular structure and activity.[14−16] Also, the spectroscopic sensing is contact-free, label-free, highly sensitive, and of high spatial resolution. The spectroscopic biosensors have demon-

Received: October 12, 2020
Revised: January 14, 2021
Published: February 1, 2021

https://dx.doi.org/10.1021/acs.nanolett.0c04067
Nano Lett. 2021, 21, 2681−2689

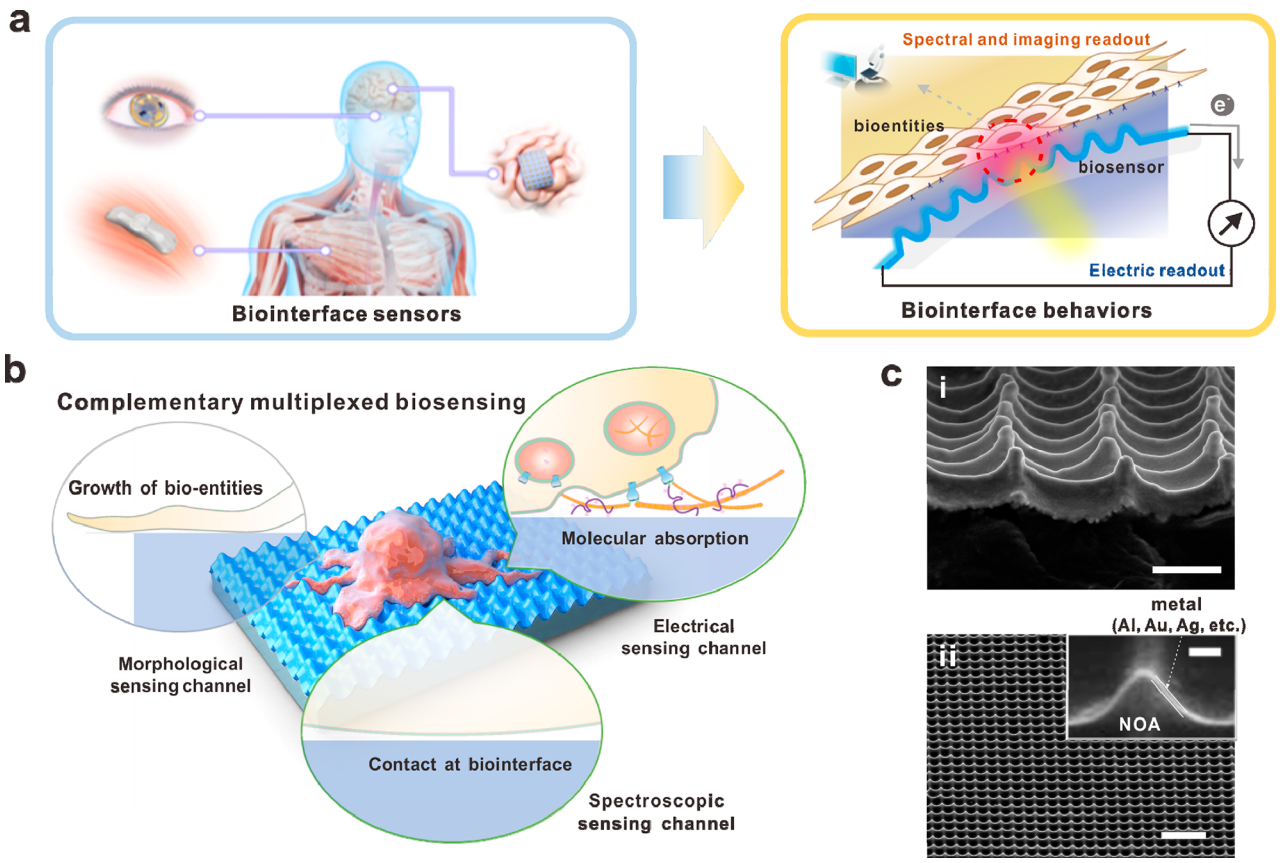

Figure 1. Complementary functions of our MMI biosensor for biointerface monitoring. (a) Typical biointerface sensors, including electrocorticography sensor, smart contact lens, and transdermal smart patch, with their main mission of monitoring the bioentity behaviors on biointerfaces. (b) Scheme of the multiplexed and complementary sensing channels, that is, electric, spectroscopic, and morphologic sensing channels for the monitoring of cell−substrate interface. (c) SEM images of our Al NPAs from the cross-section view (left) and 45° top view (right). The inset is a magnified SEM image of single pyramid. The scale bars are 1 μm, 3 μm, and 200 nm, respectively.

strated various unprecedented applications, such as the point-of-care diagnostics, imaging beyond diffraction limit, and highly miniaturized spectrometer, and so forth.[17−19] Third, the monitoring of morphologic changes (such as color and shape changes) during a biointerface process also plays a significant role such as differentiating phases of cell cycles, identifying cellular viability in biocompatibility tests, monitoring micro-environmental changes, and so forth. In the morphologic monitoring, avoiding the disturbance of the sensor's inherent color is a common but crucial challenge. Numerous efforts have been devoted to reduce the disturbance by developing transparent and colorless biosensors based on extraordinary optical transmission effect, ultrathin 2D materials, and so forth.[20,21]

In order to promote the sensing capacity of biosensors and to meet the demand of smart personalized medicine in future, a core goal in the field of biosensor is to develop multiplexed biointerface sensor, which can simultaneously possess the electric, spectroscopic, and morphologic sensing channels. However, due to inherent conflicts among these channels, such a goal is far away from realization: few of the current biointerface sensors can integrate two channels and the triplex biointerface sensor is still challenging (see summary in Table S1). Herein, by combining the advantages of metamaterials,[22,23] optical and electronic biosensing, we proposed the metaoptronic multiplexed interface (MMI) biosensor, which is built by using periodic metallic nanopyramid arrays (NPAs) supported by a flexible dielectric film. Because of the plamsonic behaviors and the conductivity of NPAs, such MMI biosensor can be colorless and transparent in the visible region, collectively providing electric, spectroscopic, and morphologic information. On the basis of the MMI biosensor, we not only develop a technique for real-time triple-monitoring of cellular dynamics but also prove the concept for powerlessly monitoring ocular dryness. With all of these remarkable performances, it is believed that our findings can motivate more researchers to explore the biosensors and pave creative avenues for nanomaterials and nanotechnologies being applied in the real world.

With the development of smart medicine and big data techniques, biointerface sensors, such as electrocorticography sensor, smart contact lens, glucometer, implanted oxygen sensor, transdermal smart patch, and so forth, have been widely applied for continuous and intimate monitoring (Figure 1a). Biointerface monitoring mainly requires data of three aspects: the molecular adsorption onto the sensor surface, the contact between the substrate sensor and the attached bioentities, and the viability/growing of the bioentity (Figure 1b). Therefore, our MMI biosensor is designed to disclose these three aspects of information simultaneously. To be specific, the NPA nanostructure (Figure 1c) of MMI was fabricated by a mature and high-throughput technique which is the combination of soft lithography and metal evaporation (using Au, Al, Ag, and so forth.). The good conductivity of NPAs makes it possible to

https://dx.doi.org/10.1021/acs.nanolett.0c04067
Nano Lett. 2021, 21, 2681−2689

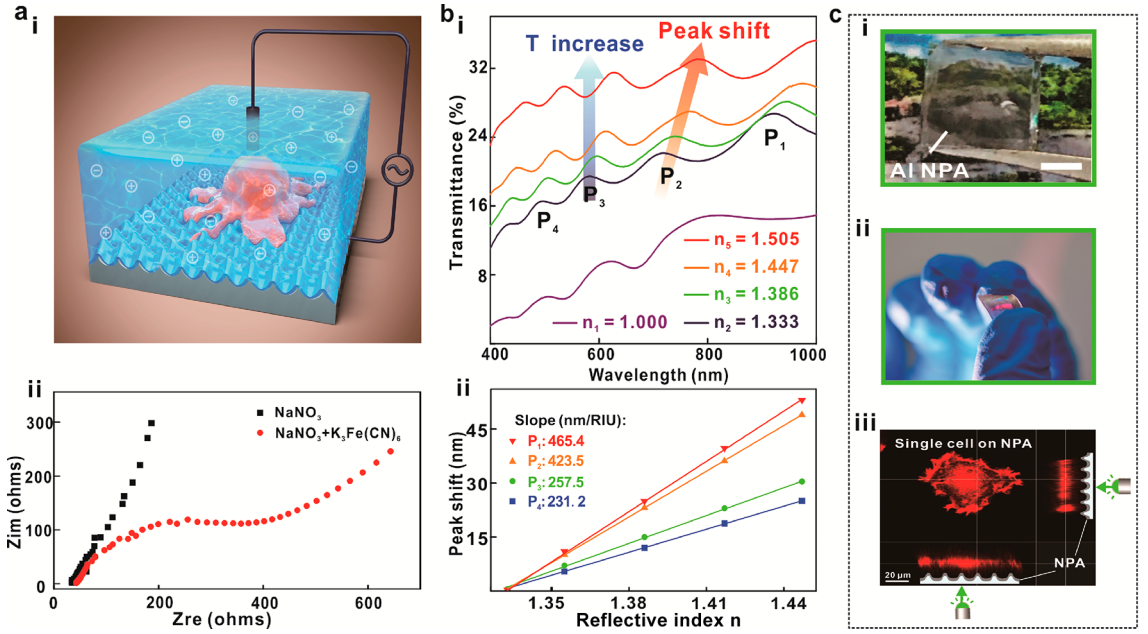

Figure 2. Triple-sensing abilities of our MMI biosensor. (a) The electrochemical sensing ability: (i) the experimental scheme; (ii) the electrochemical impedance spectroscopy (EIS) measurements using the MMI biosensor as working electrode in a $NaNO_3$ solution (black dots, with the *x*-intercept of 35), and in a mixture of $NaNO_3$ and $K_3Fe(CN)_6$ (red dots) . (b) The optical sensing ability: (i) the transmission spectra of MMI biosensor (h = 710 nm) as the environmental index increases (n_1 = 1.000, air; n_2 = 1.333, water; n_3 = 1.386, glycerol−water mixture; n_4 = 1.447, glycerol; and n_5 = 1.505, ethyl benzoate), where simultaneous transmittance increase and peak redshift are observed along with the increasing RI; (ii) the RI sensitivities of MMI biosensor at distinct peaks varying from 231.2 to 465.4 nm/RIU. (c) The colorless and flexible properties of the MMI biosensor: (i) colorless property and high transparency of MMI biosensor when it was dropped with a high-index glycerol solution; (ii) flexibility of MMI biosensor on a plastic substrate; (iii) image of *in vivo* morphology observation of a bone mesenchymal stem cell (BMSC) beside electric and optical monitoring.

serve as electric biosensors for monitoring the electron transfer of electrochemical active species and the resistance of biotissue at the electrode/solution interface. Also, our fabrication technique allows a facile and massive production of NPAs (see Methods and Figure S1 in Supporting Information), which is quite favorable for device applications. In addition, the plasmonic resonant modes of NPAs, including electric dipole (ED), magnetic dipole (MD), magnetic quadrupole (MD), and so forth, bring about several characteristic peaks in the transmission spectra (Figure S2). The location of these spectral peaks shifts with the change of environment refractive index (RI), endowing the NPAs with the capacity of spectroscopic sensing.

More importantly, the conflict between spectroscopic sensing and colorless property has been overcome by the NPAs. For the majority of spectroscopic biosensors, since their sensing mechanism is based on spectral response (i.e., spectral peak shifting with changing environment RI), they usually hold intrinsic colors and can hardly be colorless.[24−27] However, it is found that the NPAs can be colorless and transparent by increasing their environment RI. This fact may be attributed to that increasing the environment RI can decrease the polarizability (α) of NPAs,[28] and the smaller α leads to smaller optical extinction σ_{ext} ($\sigma_{ext} \propto k\ \mathrm{Im}(\alpha)$, k presents the wavevector)[29] and higher transmittance T ($\sigma_{ext} = h^2(1 - T)$, h is the period).[28] The MMI biosensor built by the NPAs enables the direct and undisturbed observations of the bioentities, so as to collect the information about the growing or viability of bioentities such as the cell viability and differentiation status. Three multiplexed channels of the MMI biosensor help to interpret the biological phenomena from different views, providing us complementary perspectives to comprehensively understand the bioentity behaviors.

The three sensing channels and their sensitivities are introduced in Figure 2. As shown in Figure 2a, the Nyquist plots of MMI biosensor in 0.1 M $NaNO_3$ electrolyte demonstrate almost a vertical line in a low-frequency region and with a low equivalent series resistance (R_s) of about 35 Ω, indicating good conductivity of our MMI biosensor. After the addition of electrochemical indicators (5 mM $Fe(CN)_6^{3-/4-}$ in this case), one can observe an obvious semicircle with a diameter of about 400 Ω in the high-frequency region, which is corresponding to the charge transfer resistance (R_{ct}).[30] The R_{ct} value of our NPAs is smaller than that of some widely used electrodes (e.g., glassy carbon, gold disk, and ITO electrode) and comparable to that of Au nanoparticle modified electrodes.[31,32] The low R_{ct} is probably due to the high conductivity and good electron-transfer properties of evaporated metals as well as the highly ordered NPA structures of our MMI biosensor,[33] which therefore could be utilized as a good alternative platform for electrical biosensors.[34]

In addition, our MMI biosensor also shows priority as an optical sensor for monitoring the RI (n) changes caused by the adsorption of analytes. As shown by the transmission spectra of the MMI biosensor under different environmental n (Figure 2b i), one can find that the transmission peaks redshift with n increasing from 1.000 to 1.505. Tracking the redshift of four peaks (i.e., P_1, P_2, P_3, P_4, at 940, 620, 525, 465 nm, respectively), it is found that the MMI biosensor can show a high RI sensitivity reaching 465.4 nm/RIU (Figure 2b ii), comparable to that of a typical plasmonic sensor in previous reports.[35] Also, it is found that the transmittance T increases

https://dx.doi.org/10.1021/acs.nanolett.0c04067
Nano Lett. 2021, 21, 2681−2689

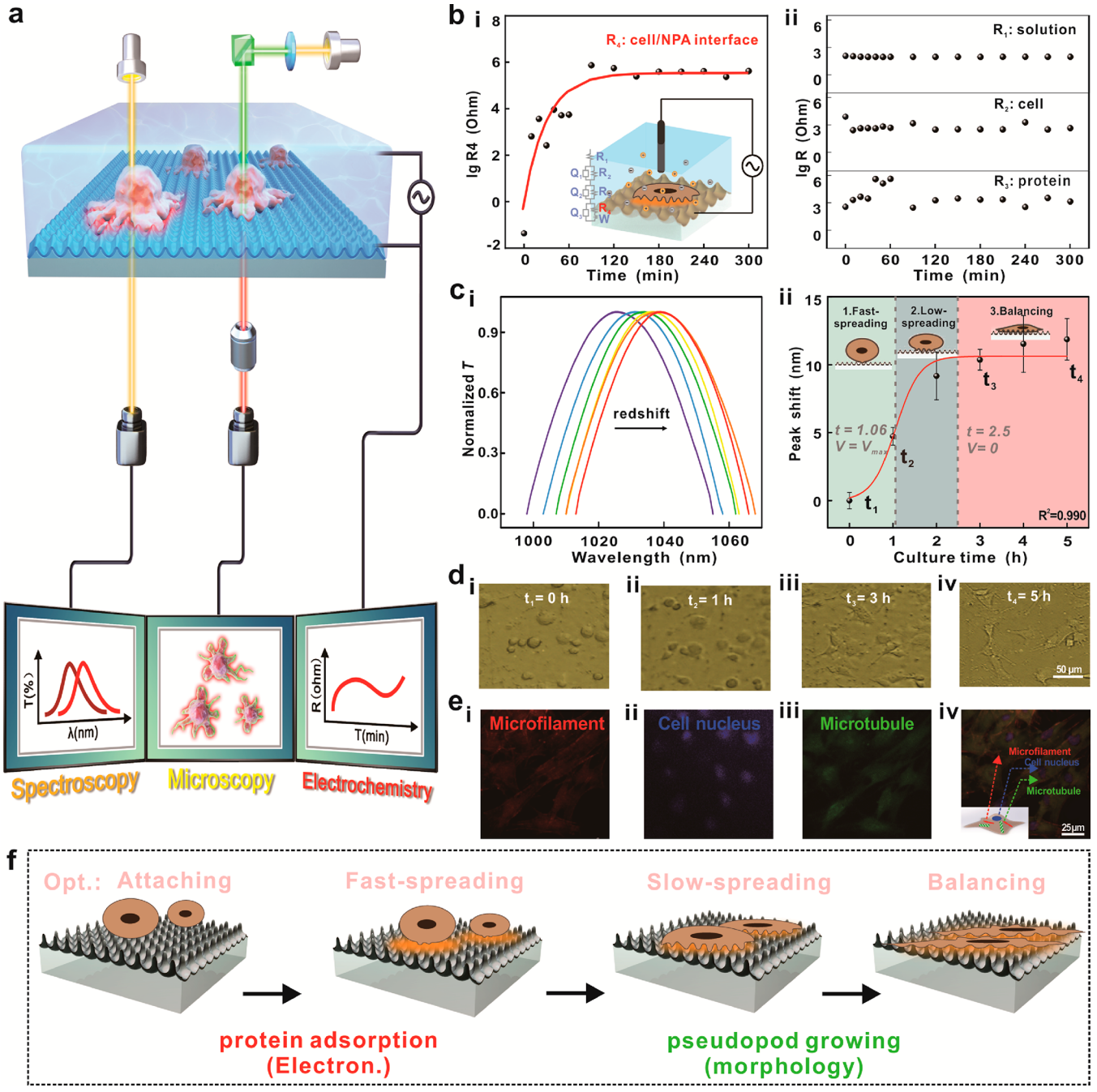

Figure 3. Complementary and multiplexed monitoring of stem cell adhesion on the MMI biosensor. (a) Scheme of the triple-monitoring for the adhesion process of BMSCs on the MMI sensor surface. (b) Electric monitoring. The relationships between the resistances of different elements and culture time. As shown in the insets of the scheme and equivalent electrical circuit mode, the elements are solution (R_1, ii top), cells (R_2, ii middle), passive adsorbed protein (R_3, ii bottom), and bio/sensor interface (R_4, i). (c) Spectral analysis. The spectral profiles of MMI biosensor at different culture time in 5.0 h (i), and the relationship between peak position and culture time (ii). This relationship fits well in a sigmoidal growth model shown as the red curve in (ii). According to the model, we can quantitatively divide the cell spreading process into three stages by the variation of peak shift velocity ($V = d\lambda/dt$): fast-spreading stage (0 to 1.06 h, V from zero to maximum), slow-spreading stage (1.06 to 2.5 h, V from maximum to zero), and balancing stage (V fluctuating around zero). (d) Morphologic observation (shape). Microscopic images of BMSCs on Al NPAs at 0, 1, 3, and 5 h (i to iv). The growing of pseudopods was clearly observed in the slow-spreading stage. (e) Morphologic observation (shape and color). Microscopic fluorescent images of multicolor labeled BMSCs on MMI biosensor, captured from the substrate side by an inverted fluorescence microscope. The nucleus (i), microfilaments (ii), and microtubules (iii) are labeled with DAPI (blue), FITC (green), and TRITC (red), respectively. Right bottom is the merged image (iv). (f) The scheme of the multistage process of cell spreading onto the MMI biosensor, interpreted by complementary sensing channels of optics, electronics, and morphology.

with the changing of environmental n, making the T another valid source of a sensing signal. This fact can further enlarge the data throughput capacity of our MMI biosensor, and the detailed sensing performances based on T variation are presented in Figure S3 (the optical sensing distance is also contained).

Furthermore, the colorless property (Figure 2c i), together with its high flexibility (Figure 2c ii), is illustrated by Figure 2c.

https://dx.doi.org/10.1021/acs.nanolett.0c04067
Nano Lett. 2021, 21, 2681−2689

The robustness of the flexible MMI sensor is proven by the results shown in Figure S4. After 150 cycles of mechanical deformation (15° bending and recovering), the MMI biosensor maintains the conductivity, spectral profile, and colorless property. These features can not only endow the MMI biosensor great potential in exploring wearable smart devices such as smart glasses or contact lenses but also enable *in situ* and real-time morphology observation during sensing, which is particularly appropriate for cell studies (Figure 2c iii).

There are always various details hiding underneath a biomedical process. Maximally revealing such biomedical details can both supplement fundamental biologic knowledge and provide alternative targets for biosensing applications. The dynamics of cell attaching and spreading is a fundamental criterion to evaluate the response of cells to environmental stimuli or substrate materials, showing great significance in drug screening,[36] oncology studies,[37] regenerative medicine,[38] cytotoxicity testing[39] and cyto-compatibility evaluation,[40] and so forth. However, due to the lack of an efficient multiplexed biosensor, quantitative and systematic investigations on cell adhesion are seldom reported.

In our experiments (Figure 3a), the bone mesenchymal stem cells (BMSCs), which are a typical group of anchorage-dependent cells, were applied. The equivalent electrical circuit model[41,42] of our system is vividly shown in the inset of Figure 3b, where R_1 to R_4 represent the resistance of solution, passive adsorbed protein, cell, and bio/sensor interface, Q_1 to Q_3 represent the constant phase element (CPE) that describes the pseudocapacitance of the above interfaces, and W is the Warburg's impedance. Any disturbance at these interfaces would cause the corresponding parameter changes. The calculated values of R_1 to R_4 at different times are given in Figure 3b. It is found that R_1 and R_2 remained almost constant at different times, indicating a stable system without obvious concentration fluctuation of electrolytes and cells during the measurement. The value of R_3 randomly changed with small variation, which is probably caused by the proteins adsorbed or desorbed onto the sensing surface. On the other hand, the bio/sensor interface (R_4) curve shows a completely different shape (Figure 3b i), experiencing a rapid increase in the initial ∼1.0 h and reaching a plateau thereafter. The increase of impedance at R_4 could be explained by the adsorption of biomass (e.g., proteins) onto the surface of the MMI biosensor, suggesting a special protein adsorption process in the first hour of cell adhesion.

Following the electric analysis, it is exciting to find that the optical monitoring can further deepen the investigation of cell adhesion dynamic by quantitatively revealing the three stages of the cell adhesion process. To be specific, during the cell adhesion, the surficial RI (n_{sur}) of MMI biosensor gradually increased from ∼1.33 (the RI of the cell culture medium) to ∼1.48 (the RI of the cell itself), resulting into an obvious redshift of extinction peaks. Without the loss of generality, one can take the extinction peak with initial center wavelength of 1026.8 nm as a typical example (Figure 3c i) and then plot its peak shift as a function of culture time (Figure 3c ii). The peak shift−time relationship can be fitted by a typical sigmoidal growth curve ($\Delta\lambda = \lambda - \lambda_0 = \Delta\lambda_0/(1 + e^{-3.6(x-1.06)})$ with a high R^2 (coefficient of determination) of 0.99, where λ_0 is the peak position at the starting point t_1, and $\Delta\lambda_0$ is the total peak shift. According to this fitted curve, one can see that the peak shift velocity ($V = d\lambda/dt$, that is, slope of this curve) increased exponentially during the first hour and then slowly decreased to zero ($V-t$ dependence curve is also presented in Figure S5). Therefore, using two time points of t = 1.06 h and t = 2.5 h, when V respectively reached its maximum and returned back to zero, the cell adhesion can be divided into three stages, which are the fast-spreading, slow-spreading, and balance stages, respectively. Since the transmittance can also be another merit for our optical biosensing, it is found that distributing the cell adhesion into three stages can also be implemented based on analysis of peak intensity (Figure S6). The results of peak location and intensity analysis agree well with each other, which not only confirms the correctness of our conclusion, but also illustrates a self-checking function of our MMI biosensor.

During the monitoring of cell behavior, *in situ* and real-time morphology observation is also crucial, because such observations can provide key information about cell viability, cell differentiating phases, bacterial contamination, and so forth. Thanks to the colorless and transparent property of our MMI biosensor, the typical cell morphologies of three adhesion stages were also recorded during the adhesion monitoring. Specifically, in the fast-spreading stage the cells exhibited a round shape (Figure 3d i and ii). In the slow-spreading stage, it is observed that pseudopods (usually two to four) were generated and those pseudopods helped the cell slowly migrate off its original location (Figure 3b iii). Lastly, when pseudopods grew slimmer (Figure 3d iv), the cells fully expanded and reached a balanced status. The recorded cell morphologies fitted well with the three stages mentioned above and vividly exhibited the nature signature of cell growing on a biosensor. Furthermore, despite these *in situ* and real-time recording of cell morphologies, the colorless property of our MMI biosensor also enables us to obtain intracellular information of cells. As a demonstration, we stained DNA, vinculin and F-actin respectively with DAPI (blue fluorescence), FITC (green fluorescence) and TRITC (red fluorescence), after the cell spreading process. Thereafter, we successfully observed the specific distributions of the cell nucleus, microtubule and microfilament correspondingly as the cells fully expanded on the MMI biosensor (Figure 3e).

On the basis of the results from complementary sensing channels, the correctness of conclusion can be strongly ensured. For example, the time of R_4 reaching its maximum is nearly the same as the ending of the fast-spreading stage which is distinguished by spectral analysis. The self-consistency of these two results guarantees the validity for each other and confirms that protein adsorption is an important character for the fast-spreading stage. In addition, the complementary MMI biosensor enables a quantitative and systematic strategy to study the cell−biomaterial interactions at the biointerface. As shown in Figure 3f, due to the combination of electric, spectroscopic, and real-time morphologic results, we not only identify the different stages of the cell adhesion, but also for the first time reveal the key features in different stages, which are the protein adsorption and pseudopod growing during the fast-spreading and slow-spreading stages, respectively.

Promoting biosensors from passive to active, as well as power-consuming to powerless, is of great significance especially for wearable biosensors. To realize these goals, the sensors are required to enable long-term, wireless, and noninvasive detections.[43−45] In fact, optical biosensors exhibit great potential for such active and powerless sensing.[46] However, their intrinsic colors limit their applications in wearable devices that need to be inconspicuously blended with

https://dx.doi.org/10.1021/acs.nanolett.0c04067
Nano Lett. 2021, 21, 2681−2689

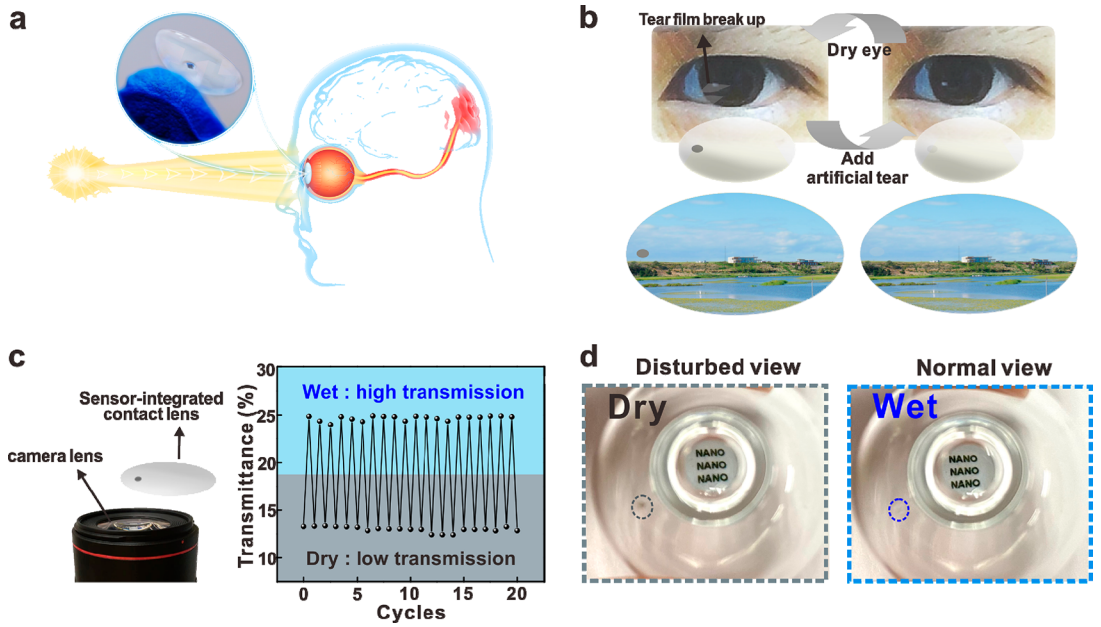

Figure 4. Colorless sensor-integrated smart contact lens for wearable and powerless sensing of ocular application. (a) Scheme illustration of the wearable and powerless smart contact lens. The MMI biosensor is integrated into a contact lens and its transmittance is dependent on the covering of tear film. The sensing process is powerless because the environmental light plays the role of light source and the retina serves as the detector. The optical signal is collected and transformed into a neuroelectric signal to bring up a sensation. (b) Scheme illustration of the sensing process of the smart contact lens. The integrated sensor can detect tear-film breakup as dry eye occurs and responds as a discernible spot within the visual field; and the disturbed view will recover upon the addition of an artificial tear. (c) The setup scheme (left) for reversibility test and the measured transmittance (right) in 20 wet−dry reversible cycles. (d) The photos captured through a model eye wearing the sensor-integrated contact lens, as the eye is in a dry or wet environment. The view is disturbed as in dry condition while remains normal when the eye is wet. The circled region indicates the location of the MMI biosensor.

a wearer's daily routine. Nevertheless, our MMI biosensor supports the advanced functions of both optical monitoring and colorless, providing a new avenue for powerlessly monitoring eye-dryness, when it was combined with a contact lens. As mentioned before, the MMI biosensor respectively exhibits high and low transmittance in wet and dry (i.e., high and low RI environments) conditions. Therefore, using the environment light (such as the sun) and human retina as the optical source and collecting CCD (i.e., charge coupled device), the MMI biosensor can actively monitor the dryness of the human eye by showing different transmittances without power supply (Figure 4a).

Specifically, during the normal wearing condition, the MMI biosensor would be embraced by a tear film with RI of ~1.34,[47] which promises it with high transmittance. Because of the high inconspicuousness, the existence of MMI biosensor can hardly be noticed if its size and location are optimized (Figure 4b). However, when the tear film breaks up, the MMI biosensor will be exposed in the air, bringing about a dramatic transmittance decrease and its appearance in the user's horizon. This situation occurs mostly after wearing contact lens for a long period without restoring the periocular tear film, which is a more serious problem nowadays due to the increasing screen time of smart devices.[48] In this situation, the presence of a negligible sensor spot in the user's vision will directly alarm the user to add artificial tear or replace/remove the contact lens, avoiding irritations and the long-term ocular diseases.

To demonstrate the proof-of-concept experiment, we integrated the MMI biosensor onto a contact lens worn by a transparent model eye and used a digital camera acting as the retina to collect the image (Figure 4c, left column). The transmittance of the sensor area shows large differences in dry and wet conditions (i.e., 13.0% and 24.8%, respectively, see Figure 4c, right column). So, under wet condition, the view is collected normally, while in dry condition a noticeable stain of gray sensor spot disturbing the natural view is captured as indicated by the circled region (Figure 4d). Here, the MMI biosensor is built up by Al deposition due to the consideration of cost efficiency. In Figure S7, a more biocompatible Au MMI biosensor with similar performance in contact lens application is also presented.

In summary, the advances of modern science rely more and more on proposing innovative ideas in either forward or inverse means. In this Letter, we introduced the idea of combining colorless metamaterials with multiplexed biosensing, and therefore got the metaoptronic multiplexed interface sensor (i.e., MMI biosensor). Our MMI biosensor can collectively perform electric, spectroscopic, and morphologic biointerface monitoring, providing complementary perspectives for comprehensively understanding the biointerface behaviors. On the basis of this MMI biosensor, a triple-monitoring technique for cell adhesion was implemented, which enables quantitative and systematic investigations on cellular dynamics. Also, a powerless sensing for ocular dryness was invented, promoting the exploration of smart biosensor with a new application. Our findings not only demonstrate the advantage of MMI biosensor, but also prove that the combination of metamaterials, optics, and electronics can be an effective direction for creating novel applications in nanoscience.

https://dx.doi.org/10.1021/acs.nanolett.0c04067
Nano Lett. 2021, 21, 2681−2689

■ ASSOCIATED CONTENT

Supporting Information

The Supporting Information is available free of charge at https://pubs.acs.org/doi/10.1021/acs.nanolett.0c04067.

Methods used in this manuscript; summary of current biointerface sensors; controlled fabrication and structural characterizations of metal NPAs; FDTD simulations on the optical behaviors of MMI biosensor; transmittance-based sensing performance of MMI biosensor; robustness of MMI biosensor; velocity−time-dependent curve for the monitoring of cell adhesion; monitoring of cell adhesion based on the change of transmission peak intensity; ocular sensing based on Au MMI biosensor (PDF)

■ AUTHOR INFORMATION

Corresponding Authors

Jianhua Zhou − *Key Laboratory of Sensing Technology and Biomedical Instruments of Guangdong Province, School of Biomedical Engineering, Sun Yat-sen University, Guangzhou 510275, China;* orcid.org/0000-0001-9895-8679; Email: zhoujh33@mail.sysu.edu.cn

Zhang-Kai Zhou − *State Key Lab of Optoelectronic Materials and Technologies, School of Physics, Sun Yat-sen University, Guangzhou 510275, China;* orcid.org/0000-0002-4341-3097; Email: zhouzhk@mail.sysu.edu.cn

Cheng-Wei Qiu − *Department of Electrical and Computer Engineering, National University of Singapore, Singapore 117583;* orcid.org/0000-0002-6605-500X; Email: chengwei.qiu@nus.edu.sg

Authors

Li Zhang − *Key Laboratory of Sensing Technology and Biomedical Instruments of Guangdong Province, School of Biomedical Engineering, Sun Yat-sen University, Guangzhou 510275, China*

Quanying Fu − *Key Laboratory of Sensing Technology and Biomedical Instruments of Guangdong Province, School of Biomedical Engineering, Sun Yat-sen University, Guangzhou 510275, China*

Yayin Tan − *Key Laboratory of Sensing Technology and Biomedical Instruments of Guangdong Province, School of Biomedical Engineering, Sun Yat-sen University, Guangzhou 510275, China*

Xuemeng Li − *Guangdong Provincial Key Laboratory of Medical Molecular Diagnosis, Department of Microbiology and Immunology, Guangdong Medical University, Dongguan 523808, China*

Yanhui Deng − *State Key Lab of Optoelectronic Materials and Technologies, School of Physics, Sun Yat-sen University, Guangzhou 510275, China*

Bin Zhou − *Key Laboratory of Sensing Technology and Biomedical Instruments of Guangdong Province, School of Biomedical Engineering, Sun Yat-sen University, Guangzhou 510275, China*

Hongqi Xia − *Key Laboratory of Sensing Technology and Biomedical Instruments of Guangdong Province, School of Biomedical Engineering, Sun Yat-sen University, Guangzhou 510275, China*

Huanjun Chen − *Guangdong Province Key Laboratory of Display Material and Technology, School of Electronics and Information Technology, Sun Yat-sen University, Guangzhou 510275, China;* orcid.org/0000-0003-4699-009X

Complete contact information is available at: https://pubs.acs.org/10.1021/acs.nanolett.0c04067

Author Contributions

Z.Z., C.Q., and J.Z. conceived the research. L.Z., Q.F., Y.T., X.L., B.Z., H.X.. and H.C. carried out the experiments. Y.D. and Z.Z. performed the theoretical calculations and analysis. L.Z., Z.Z., C.Q., and J.Z. wrote the manuscript with input from all authors. All authors contributed to the discussion and revision of the manuscript.

Notes

The authors declare no competing financial interest.

■ ACKNOWLEDGMENTS

This work was supported in part by the National Natural Science Foundation of China (Nos. 21775168, 11974437, and 91963205), the Guangdong Natural Science Funds for Distinguished Young Scholars (No. 2017B030306007), Pearl River S&T Nova Program of Guangzhou (No. 201806010033), Guangdong Special Support Program (2017TQ04C487), the Fundamental Research Funds for the Central Universities (No. 20lgzd28, 20lgzd30), and the Open Fund of IPOC (BUPT) under Grant IPOC2019A003. The work was also supported in part by the Australia-China Joint Institute for Health Technology and Innovation.

■ REFERENCES

(1) Liu, Y.; Wei, Z.; Zhou, J.; Ma, Z. Simultaneous Multi-Signal Quantification for Highly Precise Serodiagnosis Utilizing a Rationally Constructed Platform. *Nat. Commun.* **2019**, *10*, 5361.

(2) Schutgens, F.; Rookmaaker, M. B.; Margaritis, T.; Rios, A.; Ammerlaan, C.; Jansen, J.; Gijzen, L.; Vormann, M.; Vonk, A.; Viveen, M.; Yengej, F. Y.; Derakhshan, S.; de Winter-de Groot, K. M.; Artegiani, B.; van Boxtel, R.; Cuppen, E.; Hendrickx, A. P. A.; van den Heuvel-Eibrink, M. M.; Heitzer, E.; Lanz, H.; Beekman, J.; Murk, J.-L.; Masereeuw, R.; Holstege, F.; Drost, J.; Verhaar, M. C.; Clevers, H. Tubuloids Derived from Human Adult Kidney and Urine for Personalized Disease Modeling. *Nat. Biotechnol.* **2019**, *37*, 303−313.

(3) Yang, X.; Yang, M.; Pang, B.; Vara, M.; Xia, Y. Gold Nanomaterials at Work in Biomedicine. *Chem. Rev.* **2015**, *115*, 10410−10488.

(4) Kim, K.; Kim, M.-J.; Kim, D. W.; Kim, S. Y.; Park, S.; Park, C. B. Clinically Accurate Diagnosis of Alzheimer's Disease via Multiplexed Sensing of Core Biomarkers in Human Plasma. *Nat. Commun.* **2020**, *11*, 119.

(5) Wang, Y.; Wang, Y.; Zhou, F.; Kim, P.; Xia, Y. Protein-Protected Au Clusters as a New Class of Nanoscale Biosensor for Label-Free Fluorescence Detection of Proteases. *Small* **2012**, *8*, 3769−3773.

(6) Chen, G.; Roy, I.; Yang, C.; Prasad, P. N. Nanochemistry and Nanomedicine for Nanoparticle-Based Diagnostics and Therapy. *Chem. Rev.* **2016**, *116*, 2826−2885.

(7) Liu, J.; Li, F.; Wang, Y.; Pan, L.; Lin, P.; Zhang, B.; Zheng, Y.; Xu, Y.; Liao, H.; Ko, G.; Fei, F.; Xu, C.; Du, Y.; Shin, K.; Kim, D.; Jang, S.-S.; Chung, H. J.; Tian, H.; Wang, Q.; Guo, W.; Nam, J.-M.; Chen, Z.; Hyeon, T.; Ling, D. A Sensitive and Specific Nanosensor for Monitoring Extracellular Potassium Levels in the Brain. *Nat. Nanotechnol.* **2020**, *15*, 321−330.

(8) Wan, H.-Y.; Chen, J.-L.; Zhu, X.; Liu, L.; Wang, J.; Zhu, X.-M. Titania-Coated Gold Nano-Bipyramids for Blocking Autophagy Flux and Sensitizing Cancer Cells to Proteasome Inhibitor-Induced Death. *Adv. Sci.* **2018**, *5*, 1700585.

(9) Han, M.; Wang, H.; Yang, Y.; Liang, C.; Bai, W.; Yan, Z.; Li, H.; Xue, Y.; Wang, X.; Akar, B.; Zhao, H.; Luan, H.; Lim, J.; Kandela, I.;

Ameer, G. A.; Zhang, Y.; Huang, Y.; Rogers, J. A. Three-Dimensional Piezoelectric Polymer Microsystems for Vibrational Energy Harvesting, Robotic Interfaces and Biomedical Implants. *Nat. Electron.* **2019**, *2*, 26−35.
(10) Rochford, A. E.; Carnicer-Lombarte, A.; Curto, V. F.; Malliaras, G. G.; Barone, D. G. When Bio Meets Technology: Biohybrid Neural Interfaces. *Adv. Mater.* **2020**, *32*, 1903182.
(11) Lee, J. O.; Park, H.; Du, J.; Balakrishna, A.; Chen, O.; Sretavan, D.; Choo, H. A Microscale Optical Implant for Continuous in Vivo Monitoring of Intraocular Pressure. *Microsyst. Nanoeng.* **2017**, *3*, 1−9.
(12) Wang, L.; Xie, S.; Wang, Z.; Liu, F.; Yang, Y.; Tang, C.; Wu, X.; Liu, P.; Li, Y.; Saiyin, H.; Zheng, S.; Sun, X.; Xu, F.; Yu, H.; Peng, H. Functionalized Helical Fibre Bundles of Carbon Nanotubes as Electrochemical Sensors for Long-Term in Vivo Monitoring of Multiple Disease Biomarkers. *Nat. Biomed. Eng.* **2020**, *4*, 159−171.
(13) Abbott, J.; Ye, T.; Krenek, K.; Gertner, R. S.; Ban, S.; Kim, Y.; Qin, L.; Wu, W.; Park, H.; Ham, D. A Nanoelectrode Array for Obtaining Intracellular Recordings from Thousands of Connected Neurons. *Nat. Biomed. Eng.* **2020**, *4*, 232−241.
(14) Zhi, Y.; Yu, X.-C.; Gong, Q.; Yang, L.; Xiao, Y.-F. Single Nanoparticle Detection Using Optical Microcavities. *Adv. Mater.* **2017**, *29*, 1604920.
(15) Tang, S.-J.; Liu, S.; Yu, X.-C.; Song, Q.; Gong, Q.; Xiao, Y.-F. On-Chip Spiral Waveguides for Ultrasensitive and Rapid Detection of Nanoscale Objects. *Adv. Mater.* **2018**, *30*, 1800262.
(16) Huo, C.; Fong, C. F.; Amara, M.-R.; Huang, Y.; Chen, B.; Zhang, H.; Guo, L.; Li, H.; Huang, W.; Diederichs, C.; Xiong, Q. Optical Spectroscopy of Single Colloidal CsPbBr3 Perovskite Nanoplatelets. *Nano Lett.* **2020**, *20* (5), 3673−3680.
(17) Shen, Y.; Zhou, J.; Liu, T.; Tao, Y.; Jiang, R.; Liu, M.; Xiao, G.; Zhu, J.; Zhou, Z.-K.; Wang, X.; Jin, C.; Wang, J. Plasmonic Gold Mushroom Arrays with Refractive Index Sensing Figures of Merit Approaching the Theoretical Limit. *Nat. Commun.* **2013**, *4*, 2381.
(18) Yesilkoy, F.; Arvelo, E. R.; Jahani, Y.; Liu, M.; Tittl, A.; Cevher, V.; Kivshar, Y.; Altug, H. Ultrasensitive Hyperspectral Imaging and Biodetection Enabled by Dielectric Metasurfaces. *Nat. Photonics* **2019**, *13*, 390−396.
(19) Tittl, A.; Leitis, A.; Liu, M.; Yesilkoy, F.; Choi, D.-Y.; Neshev, D. N.; Kivshar, Y. S.; Altug, H. Imaging-Based Molecular Barcoding with Pixelated Dielectric Metasurfaces. *Science* **2018**, *360*, 1105−1109.
(20) Yanik, A. A.; Huang, M.; Kamohara, O.; Artar, A.; Geisbert, T. W.; Connor, J. H.; Altug, H. An Optofluidic Nanoplasmonic Biosensor for Direct Detection of Live Viruses from Biological Media. *Nano Lett.* **2010**, *10*, 4962−4969.
(21) Kuzum, D.; Takano, H.; Shim, E.; Reed, J. C.; Juul, H.; Richardson, A. G.; de Vries, J.; Bink, H.; Dichter, M. A.; Lucas, T. H.; Coulter, D. A.; Cubukcu, E.; Litt, B. Transparent and Flexible Low Noise Graphene Electrodes for Simultaneous Electrophysiology and Neuroimaging. *Nat. Commun.* **2014**, *5*, 5259.
(22) Xue, J.; Zhou, Z.-K.; Lin, L.; Guo, C.; Sun, S.; Lei, D.; Qiu, C.-W.; Wang, X.-H. Perturbative Countersurveillance Metaoptics with Compound Nanosieves. *Light: Sci. Appl.* **2019**, *8*, 101.
(23) Yue, F.; Wen, D.; Zhang, C.; Gerardot, B. D.; Wang, W.; Zhang, S.; Chen, X. Multichannel Polarization-Controllable Superpositions of Orbital Angular Momentum States. *Adv. Mater.* **2017**, *29* (15), 1603838.
(24) Zhou, Z.-K.; Liu, J.; Bao, Y.; Wu, L.; Png, C. E.; Wang, X.-H.; Qiu, C.-W. Quantum Plasmonics Get Applied. *Prog. Quantum Electron.* **2019**, *65*, 1−20.
(25) Xue, J.; Zhou, Z.-K.; Wei, Z.; Su, R.; Lai, J.; Li, J.; Li, C.; Zhang, T.; Wang, X.-H. Scalable, Full-Colour and Controllable Chromotropic Plasmonic Printing. *Nat. Commun.* **2015**, *6*, 8906.
(26) Anker, J. N.; Hall, W. P.; Lyandres, O.; Shah, N. C.; Zhao, J.; Van Duyne, R. P. Biosensing with Plasmonic Nanosensors. *Nat. Mater.* **2008**, *7*, 442−453.
(27) Akselrod, G. M.; Argyropoulos, C.; Hoang, T. B.; Ciracì, C.; Fang, C.; Huang, J.; Smith, D. R.; Mikkelsen, M. H. Probing the Mechanisms of Large Purcell Enhancement in Plasmonic Nanoantennas. *Nat. Photonics* **2014**, *8*, 835−840.
(28) Auguié, B.; Barnes, W. L. Collective Resonance in Gold Nanoparticle Arrays. *Phys. Rev. Lett.* **2008**, *101*, 143902.
(29) García-Etxarri, R.; Gómez-Medina, R.; Froufe-Pérez, L. S.; López, C.; Chantada, L.; Scheffold, F.; Aizpurua, J.; Nieto-Vesperinas, N.; Sáenz, J. J. Strong Magnetic Response of Submicron Silicon Particles in the Infrared. *Opt. Express* **2011**, *19*, 4815−4826.
(30) Bertok, T.; Lorencova, L.; Chocholova, E.; Jane, E.; Vikartovska, A.; Kasak, P.; Tkac, J. Electrochemical Impedance Spectroscopy Based Biosensors: Mechanistic Principles, Analytical Examples and Challenges towards Commercialization for Assays of Protein Cancer Biomarkers. *ChemElectroChem* **2019**, *6*, 989−1003.
(31) Rostamabadi, P. F.; Heydari-Bafrooei, E. Impedimetric Aptasensing of the Breast Cancer Biomarker HER2 Using a Glassy Carbon Electrode Modified with Gold Nanoparticles in a Composite Consisting of Electrochemically Reduced Graphene Oxide and Single-Walled Carbon Nanotubes. *Microchim. Acta* **2019**, *186*, 495.
(32) Lacina, K.; Sopoušek, J.; Čunderlová, V.; Hlaváček, A.; Václavek, T.; Lacinová, V. Biosensing Based on Electrochemical Impedance Spectroscopy: Influence of the Often-Ignored Molecular Charge. *Electrochem. Commun.* **2018**, *93*, 183−186.
(33) Quan, X.; Fischer, L. M.; Boisen, A.; Tenje, M. Development of Nanoporous Gold Electrodes for Electrochemical Applications. *Microelectron. Eng.* **2011**, *88*, 2379−2382.
(34) Luo, X.; Davis, J. J. Electrical Biosensors and the Label Free Detection of Protein Disease Biomarkers. *Chem. Soc. Rev.* **2013**, *42*, 5944−5962.
(35) Mayer, K. M.; Hafner, J. H. Localized Surface Plasmon Resonance Sensors. *Chem. Rev.* **2011**, *111*, 3828−3857.
(36) Kenny, H. A.; Lal-Nag, M.; White, E. A.; Shen, M.; Chiang, C.-Y.; Mitra, A. K.; Zhang, Y.; Curtis, M.; Schryver, E. M.; Bettis, S.; Jadhav, A.; Boxer, M. B.; Li, Z.; Ferrer, M.; Lengyel, E. Quantitative High Throughput Screening Using a Primary Human Three-Dimensional Organotypic Culture Predicts in Vivo Efficacy. *Nat. Commun.* **2015**, *6*, 6220.
(37) Horzum, U.; Ozdil, B.; Pesen-Okvur, D. Differentiation of Normal and Cancer Cell Adhesion on Custom Designed Protein Nanopatterns. *Nano Lett.* **2015**, *15*, 5393−5403.
(38) Ye, K.; Wang, X.; Cao, L.; Li, S.; Li, Z.; Yu, L.; Ding, J. Matrix Stiffness and Nanoscale Spatial Organization of Cell-Adhesive Ligands Direct Stem Cell Fate. *Nano Lett.* **2015**, *15*, 4720−4729.
(39) Tong, F.; Lian, Y.; Zhou, H.; Shi, X.; He, F. Multichannel Series Piezoelectric Quartz Crystal Cell Sensor for Real Time and Quantitative Monitoring of the Living Cell and Assessment of Cytotoxicity. *Anal. Chem.* **2014**, *86*, 10415−10421.
(40) Place, E. S.; Evans, N. D.; Stevens, M. M. Complexity in Biomaterials for Tissue Engineering. *Nat. Mater.* **2009**, *8*, 457−470.
(41) Astorga, S. E.; Hu, L. X.; Marsili, E.; Huang, Y. Electrochemical Signature of Escherichia Coli on Nickel Micropillar Array Electrode for Early Biofilm Characterization. *ChemElectroChem* **2019**, *6*, 4674−4680.
(42) Soussi, I.; Mazouz, Z.; Collart-Dutilleul, P. Y.; Echabaane, M.; Martin, M.; Cloitre, T.; M'ghaieth, R.; Cuisinier, F. J. G.; Cunin, F.; Gergely, C.; Othmane, A. Electrochemical and Optical Investigation of Dental Pulp Stem Cell Adhesion on Modified Porous Silicon Scaffolds. *Colloids Surf., B* **2019**, *181*, 489−497.
(43) Park, J.; Kim, J.; Kim, S.-Y.; Cheong, W. H.; Jang, J.; Park, Y.-G.; Na, K.; Kim, Y.-T.; Heo, J. H.; Lee, C. Y.; Lee, J. H.; Bien, F.; Park, J.-U. Soft, Smart Contact Lenses with Integrations of Wireless Circuits, Glucose Sensors, and Displays. *Sci. Adv.* **2018**, *4*, eaap9841.
(44) Han, S.; Kim, J.; Won, S. M.; Ma, Y.; Kang, D.; Xie, Z.; Lee, K.-T.; Chung, H. U.; Banks, A.; Min, S.; Heo, S. Y.; Davies, C. R.; Lee, J. W.; Lee, C.-H.; Kim, B. H.; Li, K.; Zhou, Y.; Wei, C.; Feng, X.; Huang, Y.; Rogers, J. A. Battery-Free, Wireless Sensors for Full-Body Pressure and Temperature Mapping. *Sci. Transl. Med.* **2018**, *10*, eaan4950.
(45) Boutry, C. M.; Beker, L.; Kaizawa, Y.; Vassos, C.; Tran, H.; Hinckley, A. C.; Pfattner, R.; Niu, S.; Li, J.; Claverie, J.; Wang, Z.; Chang, J.; Fox, P. M.; Bao, Z. Biodegradable and Flexible Arterial-

https://dx.doi.org/10.1021/acs.nanolett.0c04067
Nano Lett. 2021, 21, 2681−2689

Pulse Sensor for the Wireless Monitoring of Blood Flow. *Nat. Biomed. Eng.* **2019**, *3*, 47−57.
(46) Yamagishi, K.; Kirino, I.; Takahashi, I.; Amano, H.; Takeoka, S.; Morimoto, Y.; Fujie, T. Tissue-Adhesive Wirelessly Powered Optoelectronic Device for Metronomic Photodynamic Cancer Therapy. *Nat. Biomed. Eng.* **2019**, *3*, 27−36.
(47) Lu, H.; Wang, M. R.; Wang, J.; Shen, M. Tear Film Measurement by Optical Reflectometry Technique. *J. Biomed. Opt.* **2014**, *19*, 027001.
(48) Rabiah, N. I.; Scales, C. W.; Fuller, G. G. The Influence of Protein Deposition on Contact Lens Tear Film Stability. *Colloids Surf., B* **2019**, *180*, 229−236.

https://dx.doi.org/10.1021/acs.nanolett.0c04067
Nano Lett. 2021, 21, 2681−2689